Acta Oceanol. Sin., 2020, Vol. 39, No. 9, P. 5–17
https://doi.org/10.1007/s13131-020-1643-8
http://www.hyxb.org.cn
E-mail: hyxbe@263.net

Characterization of the unprecedented polynya events north of Greenland in 2017/2018 using remote sensing and reanalysis data

Ruibo Lei[1]*, Dawei Gui[1, 2], Zhuoli Yuan[1], Xiaoping Pang[2], Ding Tao[1], Mengxi Zhai[1]

[1] MNR Key Laboratory for Polar Science, Polar Research Institute of China, Shanghai 200136, China

[2] Chinese Antarctic Center of Surveying and Mapping, Wuhan University, Wuhan 430072, China

Received 22 May 2019; accepted 20 August 2019

Abstract

Based on an ice concentration threshold of 90%, it has been identified that two polynya events occurred in the region north of Greenland during the 2017/2018 ice season. The winter event lasted from February 20 to March 3, 2018 and the summer event persisted from August 2 to September 5, 2018. The minimum ice concentration derived from Advanced Microwave Scanning Radiometer 2 (AMSR2) observations was 72% and 65% during the winter and summer events, respectively. The occurrence of both events can be related to strengthened southerly winds associated with an increased east-west zonal surface level air pressure gradient across the north Greenland due to perturbation of mid-troposphere polar vortex. The relatively warm air temperature during the 2017/2018 freezing season in comparison with previous years, together with the occurrence of the winter polynya, formed favourable pre-conditions for ice field fracturing in summer, which promoted the formation of the summer polynya. Diminished southerly winds and increased cover of new ice over the open water were the dominant factors for the disappearance of the winter polynya, whereas increased ice inflow from the north was the primary factor behind the closure of the summer polynya. Sentinel-1 Synthetic Aperture Radar (SAR) images were found better suited than AMSR2 observations for quantification of a new ice product during the polynya event because the SAR images have high potential for mapping of different sea ice regimes with finely spatial resolution. The unprecedented polynya events north of Greenland in 2017/2018 are important from the perspective of Arctic sea ice loss because they occurred in a region that could potentially be the last "Arctic sea ice refuge" in future summers.

Key words: sea ice, ice concentration, ice motion, polynya, Greenland, Arctic Ocean

Citation: Lei Ruibo, Gui Dawei, Yuan Zhuoli, Pang Xiaoping, Tao Ding, Zhai Mengxi. 2020. Characterization of the unprecedented polynya events north of Greenland in 2017/2018 using remote sensing and reanalysis data. Acta Oceanologica Sinica, 39(9): 5–17, doi: 10.1007/s13131-020-1643-8

1 Introduction

Polynyas are regions of open water and/or thin ice that occur within sea ice zones at locations where a more consolidated and thicker ice cover might be expected climatologically (Martin, 2001). They differ from leads, which are linear openings that appear ephemerally, and they tend to occur randomly from a spatial perspective (Tamura and Ohshima, 2011). Polynyas have generally been categorized into latent- and sensible-heat types based on their mechanisms of formation and maintenance. Latent-heat polynyas occur in regions where ice has been removed by winds and/or ocean currents (Barber and Massom, 2007). Sensible-heat polynyas occur in regions where ice formation has been prevented because of the transport of oceanic heat to the surface by upwelling, vertical mixing, or deep-ocean convection (Comiso and Gordon, 1996).

Similar to those over the leads, atmosphere–ocean heat fluxes through a polynya are several orders of magnitude greater than through the pack ice zone (Maykut, 1982). Thus, they dominate the regional heat budget and the ocean-to-atmosphere losses of moisture and heat (Morales Maqueda et al., 2004), which can result in warming of the air column above polynyas and modification of the mesoscale atmospheric circulation (Gallée, 1997). Latent-heat polynyas have high rates of ice production and they have been described as "ice factories" because of the rapid loss of heat from open water or thin ice to the atmosphere (Martin et al., 2005; Gutjahr et al., 2016). Brine rejection during the formation of frazil ice within polynyas increases the salinity of the upper ocean, which has an effect on local vertical mixing (Dmitrenko et al., 2005; Krumpen et al., 2011) and the large-scale baroclinic circulation (Tamura and Ohshima, 2011; Ohshima et al., 2016). It has been suggested that the Arctic halocline might be maintained by advection of cold saline water formed because of sea ice growth within polynyas over continental shelves (Cavalieri and Martin, 1994). Polynya size ranges from 10 km^2 to 10^5 km^2, which is a scale much greater than leads. Thus, from an ecological point of view, polynyas could be defined as "oases" because they enable birds and mammals to overwinter at high latitudes and they encourage enhanced primary production in the spring, especially those polynyas in the Bering Sea in Arctic and the Ross Sea in Antarctica (Barber and Massom, 2007). From a perspective of biogeochemical cycle, polynyas could be considered as a window for the atmosphere–ocean gas exchange. It has been es-

Foundation item: The National Key Research and Development Program of China under contract Nos 2018YFA0605903 and 2016YFC1402702; the National Natural Science Foundation of China under contract Nos 41722605 and 41976219.
*Corresponding author, E-mail: leiruibo@pric.org.cn

timated that winter CO_2 exchange through leads and small polynya openings accounts for >50% of the total CO_2 uptake in the Cape Bathurst polynya region of the Beaufort Sea (Else et al., 2013).

In the Arctic, polynyas often occur in relation to ice or land bridges in the upstream areas of winds or currents and/or enhanced oceanic flow through straits. Generally, polynyas are not particularly widespread around the Greenland (Barber and Massom, 2007). The North Water (NOW) polynya occurred south of the Nares Strait between Ellesmere Island and northwestern Greenland, where the most important factor in keeping the polynya open is mechanical removal of ice by currents and winds south of an ice bridge that forms across the north of Nares Strait in winter (Tamura and Ohshima, 2011). The Northeast Water polynya occurred to the northwest of Greenland, where interaction of the northward coastal current with the Norskeøb Ice Barrier is a major factor in creating the polynya (Dmitrenko et al., 2015). The oldest and thickest sea ice of the Arctic Ocean generally remains within the region between the Canadian Arctic Archipelago, Greenland, and the North Pole (e.g., Lindsay and Schweiger, 2015). In this region, surface air temperature also is lower than other regions of the Arctic Ocean in the climatology (Moore, 2016). Thus, in the region north of Greenland between the Lincoln Sea and the Fram Strait, the occurrence of polynyas prior to winter 2017–2018 has not been reported (Moore et al., 2018).

As an extension of a study by Moore et al. (2018), we further analysed the polynya processes north of Greenland that occurred to the north of Greenland in winter 2017–2018. In contrast to the study by Moore et al. (2018), rather than treat the polynya processes as isolated events, this study considered them in relation to the atmospheric and ice conditions throughout the entire ice season. Thus, the pre-conditions of atmospheric forcing and ice conditions necessary for polynya formation were assessed. The polynya reoccurred north of Greenland in summer 2018. Thus, the potential effects of the winter icescape on the formation of summer polynya were also investigated. The high-resolution optical images derived from the Moderate Resolution Imaging Spectroradiometer (MODIS) and the Synthetic Aperture Radar (SAR) images acquired from Sentinel-1 were used to determine the finely surface regimes, i.e., the spatially distributions of old thick ice, new thin ice, and open water, during the polynya processes.

2 Data and methods

As shown in Fig. 1, compared to the study region defined by Moore et al. (2018), our defined study region extends westward to the Nares Strait because the part of the Lincoln Sea to the north of the Nares Strait also exhibited low sea ice concentration in summer 2018. The northern, western, and eastern boundaries of the study region were defined along the latitude or longitude lines of 85°N, 60°W, and 12°W with lengths of 450 km, 297 km and 369 km, respectively. The southern boundary was defined as the connection of the coastal capes north of Greenland. The area of the study region was 11.9×10^4 km^2. We defined the study period as extending from October 2017 to September 2018 to characterize the annual cycle of ice conditions and atmospheric forcing related to the polynya processes within the study region.

The formation of the polynya north of Greenland during February–March of 2018 can be attributed to the local abnormal meridional wind (Moore et al., 2018). Futhermore, the meridional wind is related closely to the zonal gradient of air pressure (e.g., Kwok, 2005). Therefore, we calculated the surface level pressure (SLP) gradient from point A (80°N, 90°W) located in Ellesmere to point B (80°N, 15°E) in Svalbard. Sea ice concentration within the study region was derived from the Advanced Microwave Scanning Radiometer 2 (AMSR2) product, with spatial resolution of 6.25 km$^2\times$6.25 km^2 (Spreen et al., 2008). We used the AMSR2 product because it has higher spatial resolution than other passive microwave products (e.g., the SMMR-SSMIS product). Through combination with data derived from its predecessor (AMSR-E), we obtained a quasi-continuous time series of ice concentration from 2002–2018, with the exception of 2011. To assess the openness of the polynya, the ice condition during the polynya processes of the 2017/2018 ice season was compared with the same period in other years. During winter polynya processes, Sentinel-1 C-band SAR images were obtained from 11 February to 5 March 2018, which covered the study region partly or completely each day with two or three overlapping scenes. The Sentinel-1 SAR images are HH polarized and they have spatial resolution of approximately 90 m×90 m. In the case of radar frequency, C-band is preferred for the purpose of discrimination between thin ice and thick ice (Dierking, 2013) because short wavelengths cannot easily penetrate sea ice. The HH polarization is better than others because ocean clutter (e.g., rougness due to the wave) is more suppressed at HH polarization (Dierking, 2013). In comparison with the AMSR2 passive microwave observations, the SAR images can help quantify the new ice product within the polynya because the backscattering characteristics of thick ice, new thin ice, and open water are very different. The incidence angle of SAR image used here ranged from 24° to 45°. Thus the greyscale and brightness of SAR image for the

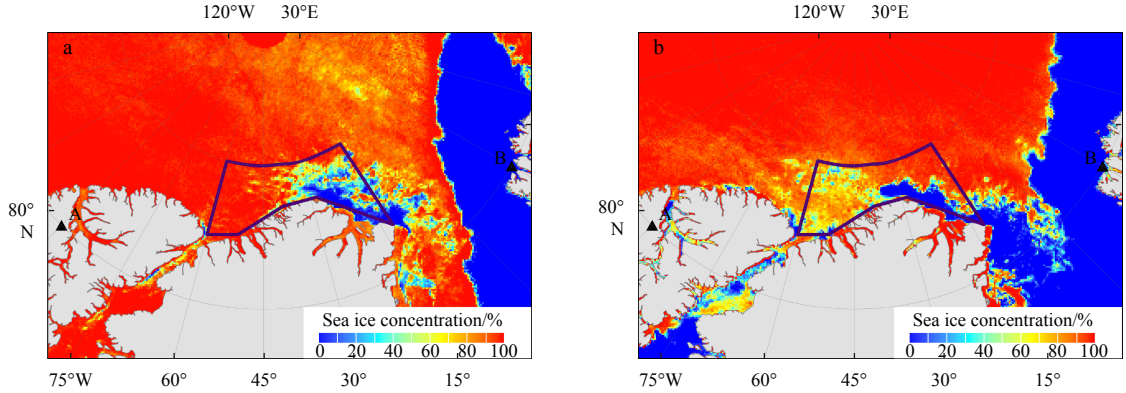

Fig. 1. Sea ice concentration on February 26 (a) and August 8, 2018 (b). Dark blue line indicates the study region and black triangles denote locations used to calculate the zonal SLP gradient.

same object would change from scene to scene, which would significantly affect the results of surface classification (e.g., Hong and Yang, 2018). Thus, we adjusted the thresholds of each scene of image repeatedly to make the segmentation result more consistent with the result classified manually. We also noted that the floe surface might be very inhomogeneous because of ridges, which would result in some discrete speckles over the SAR images. Thus, after initial image segmentation, these grey or black speckles within the contours of ice floes were removed by dissolving spots gradually from floe perimeter to inside prior to the determination of the fractions of thick ice, thin ice, and open water. Among the objects, it is most difficult to discriminate the thin ice from open water because the backscattering characteristics of thin ice are very close to ocean clutter. However, the advantages for our case study included (1) the wind fetch was very limited because open waters are discontinuous during the winter polynya event, which prevented the occurrence of strong waves and large roughness over water surface; and (2) the surface air temperature remained well below the freezing point of seawater during the winter polynya event, which would promote the formations of frazil and grease ice over the open waters immediately just after the occurring of opening, and would suppress the surface roughness over waters effectively and make sure the distinctly contrast of backscattering properties between thin ice and open water. The smooth temporal changes in our derived area fraction of thin ice make us very confident about the results of segmentation of surface regimes because the appearance of ocean clutters is very random. The low contrast of backscattering properties between ice and water because of the melt of ice surface and the relatively large roughness of water surface makes us give up using summer SAR image to classify the surface regimes.

During the summer polynya event, MODIS optical images with spatial resolution of 250 m, collected on eight selected days during August 1 to September 19, 2018 when cloud contamination was low, were used to determine the changes in ice conditions because floe outlines were clearer in the optical images in comparison with the summertime SAR images. The MODIS images were synthesized using the data of Band 1 (620–670 nm), Band 4 (545–565 nm) and Band 5 (1 230–1 250 nm).

Reanalysis data of SLP, 10-m wind, and 2-m air temperature derived from the ECMWF ERA-Interim product (Dee et al., 2011) were used to characterize the local surface atmospheric forcing. ERA-Interim data of 500-hPa geopotential height were used to assess the influence of the mid-tropospheric flow on surface atmospheric conditions. The daily ice motion product provided by the National Snow and Ice Data Centre (NSIDC) was used to estimate the ice flow across the boundaries of the study region to estimate the dynamic budget of sea ice. Among four common-used sea ice motion products (OSI SAF, CERSAT, NSIDC, and ice drift vectors from Kimura et al. (2013)), OSI SAF and NSIDC revealed relatively small uncertainty compared to other two products especially in the regions with high sea ice concentration (Sumata et al., 2014). During the summer, the uncertainty of NSIDC product ranges from 1.0 cm/s to 2.0 cm/s, which would be reduced significantly during winter because of the increased ice concentration and the decreased ice speed (Sumata et al., 2015). Furthermore, the NSIDC data are available through the year. Thus, we selected the NSIDC product of ice motion to characterize the annual cycle of ice velocity across the study region.

3 Results

3.1 *Sea ice concentration*

Based on the AMSR2 passive microwave observations, two polynya events were identified to have occurred during the ice season from October 2017 to September 2018. A threshold of 90% for the spatially averaged ice concentration within the study region was used to establish that the winter polynya event lasted from February 20 to March 3, 2018 and that the summer polynya event persisted from August 2 to September 5, 2018 (Fig. 2). Here we used a cutoff of 90% for the ice concentration to define the polynya event because this cutoff is just below the 2002–2018 average during the same period (i.e., 90.8%) by one standard deviation. Generally, a polynya event is defined as a process occurring in the ice freezing season. However, because the study region is generally covered by the oldest and thickest ice within the Arctic Ocean, ice concentration usually remains at a high level in summer (Lange et al., 2019). During the summers of 2002–2017, ice concentration within the study region almost never decreased to <85%. Thereby, the process with low ice concentration during summer 2018 was also defined as a polynya event here.

During the winter polynya event, the ice concentration decreased from near 100% on February 15 to 72% by February 26, 2018, with the minimum less than the average by two standard deviations. This minimum was also the lowest value for all the freezing seasons during 2002–2018. However, this polynya event only lasted a very short time and the ice concentration increased to near 100% again by March 7, 2018. During the winter polynya event from February 20 to March 3, 2018, the average ice concentration was 82%, which was 17% lower than the 2002–2018 average (Table 1). From May 2018 onwards, the ice concentration exhibited reasonably large fluctuation, which implies the cohesive-

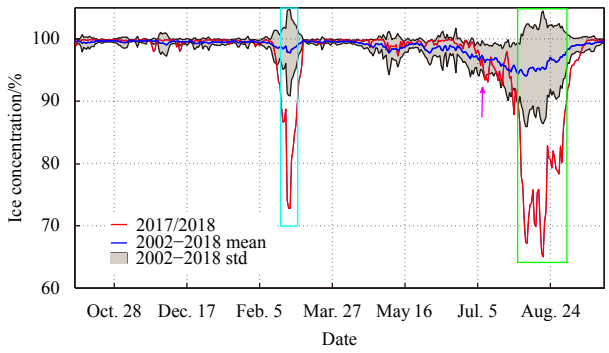

Fig. 2. Spatial average ice concentration within the study region in the 2017–2018 ice season, and the multiyear average and standard deviation (2002–2018) during the same period. Cyan and green rectangles denote the periods of the polynya events. Purple arrow denotes the day on which the SLP decreased to the second lowest value during the study period.

Table 1. Statistics of environmental parameters during the winter and summer polynya events, with the anomalies shown in parentheses

	Winter event	Summer event
Start time	Feb. 20	Aug. 2
End time	Mar. 3	Sep. 5
Average ice concentration/%	82 (–17)	77 (–19)
Average SLP gradient/hPa	–14 (–23)	–2 (–1)
Average northward wind speed/m·s^{-1}	4.3 (5.2)	1.4 (1.0)
Average northward ice speed/km·d^{-1}	2.6 (4.0)	0.3 (1.1)
Average air temperature/°C	–14.2 (14.0)	0.2 (0.5)

ness among the floes decreased gradually with summer approaching. The ice concentration decreased rapidly from July 5, 2018 onward to reach 67% by August 8, 2018, which was also lower than the 2002–2018 climatology by more than two standard deviations. The ice concentration increased rapidly from August 19, 2018 onward and it reached a value of >90% by September 5 and >98% by September 15, 2018. During the summer polynya event, the average ice concentration was 77%, which was 19% lower than the 2002–2018 average. Thus, this event can increase the absorption of solar radiation by the ice-ocean system by 17% on the basis of assumed ice and open-water albedos of 0.7 and 0.1 (e.g., Lei et al., 2016b), respectively, and neglected interannual change in the incident solar radiation. Thus, the summer polynya event would promote the melt of sea ice.

Although the Sentinel-1 SAR images did not cover the study region completely throughout the entire winter polynya event, they always covered the central part of the study region, i.e., 84°–85°N, 25°–45°W, representing an area of 2.4×10^4 km^2. Thus, we used the SAR images of this sub-region to identify the area fractions of thick ice, new thin ice, and open water and to estimate the new ice production during the polynya process. As shown in Fig. 3, the original SAR images were segmented into three types of object based on their greyscale values corresponding to the backscattering properties of targets, with white, grey and blue denoting thick ice, new thin ice, and open water, respectively. On February 17, 2018, some flow leads occurred along the northern shore of Greenland and they extended northwestward. However, the sea ice concentration remained high within the sub-region, as reflected by the value of 97% derived from both the AMSR2 and the SAR images (Fig. 4). The diameter of most floes was >50 km. On February 22, 2018, a vast tract of new thin ice occurred over the open water in the southeastern part of the sub-region, where grey/white stripes of high radar backscatter appeared indicating new ice in the polynya area. The area fraction of thin ice identified from the SAR images increased to 8% by that time. The fragmentation of ice floes on that day was more obvious compared with February 17, 2018. A large number of ice floes with diameter of <40 km appeared in the western part of the sub-region because of tensile and shear failure of the floes. On February 27, 2018, the fragmentation of ice floes developed further and the diameter of most floes was <20 km. Note, the small cracks through the floes still cannot be identified using the SAR images because of the limited spatial resolution. Thus, the dimensions of floes would be overestimated here. The real fragmentation of ice floes should be more serious. The new ice was widespread, especially in the eastern part of the sub-region. The area fraction of thin ice increased to 43%. Because only a small part of the new thin ice could be identified by the AMSR2 observations in the initial stage, the AMSR2 ice concentration was obviously smaller than the ice concentration determined using the SAR images from February 23 to March 3, 2018. For example, on February 27, 2018, the ice concentration in the sub-region as derived from AMSR2 and SAR was 73% and 93%, respectively.

The time series of the area fractions for various objects (Fig. 4) show that the concentration of thick ice within the sub-region decreased rapidly from 93% on February 20 to 51% by February 25, 2018, which was almost synchronous with the changes in the AMSR2 ice concentration. Correspondingly, the area fraction of new thin ice obtained from the SAR images increased from 5% to 47%. This implies that the decreased AMSR2 ice concentration could be attributed to the loss of the original thick ice, and that most new ice could not be identified by the AMSR2 observations in the initial stage. From February 25 to March 4, 2018, the AMSR2 ice concentration increased rapidly from 51% to 93%. However, the area fraction of thick ice identified from the SAR images increased only slightly from 51% to 65% and the area of thin ice decreased slightly from 47% to 29%. It can be deduced that the increased AMSR2 ice concentration was attributable primarily to thickening of new ice over the polynya and secondarily to the inflow of thick ice. As shown in Fig. 3h, some new ice in the eastern part of the sub-region started to exhibit the backscattering characteristics of thick ice on March 3, 2018 with whitening of the greyscale. Comparison of AMSR2 and SAR observations indicates that passive microwave observations are insufficient to characterize the polynya process, especially for the assessment of the new ice product. Conversely, the Sentinel-1 SAR images show great potential from this perspective. We also acknowledge that the influence of ocean clutter on the discrimination of thin ice should be further assessed in the future by combining the SAR images obtained from other satellite sources or aerial observation (e.g., Dierking, 2010). However, we argue that the data is reasonably acceptable because the estimated area fraction of thin ice changed smoothly day by day. The influence of ocean clutter, if it cannot be ignored, should have a significant temporal fluctuation because it was strongly dependent on the wind regime and the geometric characteristics of wind fetch, both of which have great randomness.

On August 1, 2018, although the ice concentration remained high, i.e., the AMSR2 value was 91%, the ice floes within the study region exhibited a high degree of fragmentation with very few ice floes having a diameter of >30 km. We speculate this phenomenon could be attributed to the winter polynya process because a large number of crushed ice floes were formed during the winter polynya event. Although the winter polynya event lasted for only approximately 15 d, and the refreezing occurred very rapidly in early March 2018, the new ice should have experienced reasonably little thermodynamic thickening because of its short growing season. During deformation of an ice field under atmospheric or oceanic forcing, new ice acts as a mechanically fragile zone. The summer polynya was evident within the MODIS images from August 6 to September 1, 2018 (Fig. 5), which agrees with the AMSR2 observations, with ice concentration ranging from 64% to 83%. Especially on August 19, 2018, large areas of open water appeared off the northern Greenland. The AMSR2 ice concentration within the study region decreased to an annual minimum of 64% by then, which also was the minimum observed in 2002–2018. During September 1–9, 2018, the ice concentration within the study region increased gradually, with the AMSR2 concentration increasing from 80% to 95%, which indicated the closure of the summer polynya. From the MODIS images, we also found that the size of the ice floes within the study region increased markedly during September 6–19, 2018 because of the replacement of small floes by larger floes from the north. The original small floes were removed because of southward advection into either the Fram Strait or the Nares Strait.

3.2 *Surface atmospheric circulation*

As shown in Fig. 6, the difference in SLP between 90°W and 15°E at 80°N in the 1979–2018 climatology was always positive from October to mid-June but near neutral from then onward. The positive SLP gradient between these two points implies a southward flow of ice across the study region. Thus, the climatological seasonality of this SLP gradient was coincident with the observed seasonality of Arctic sea ice outflow through the Fram

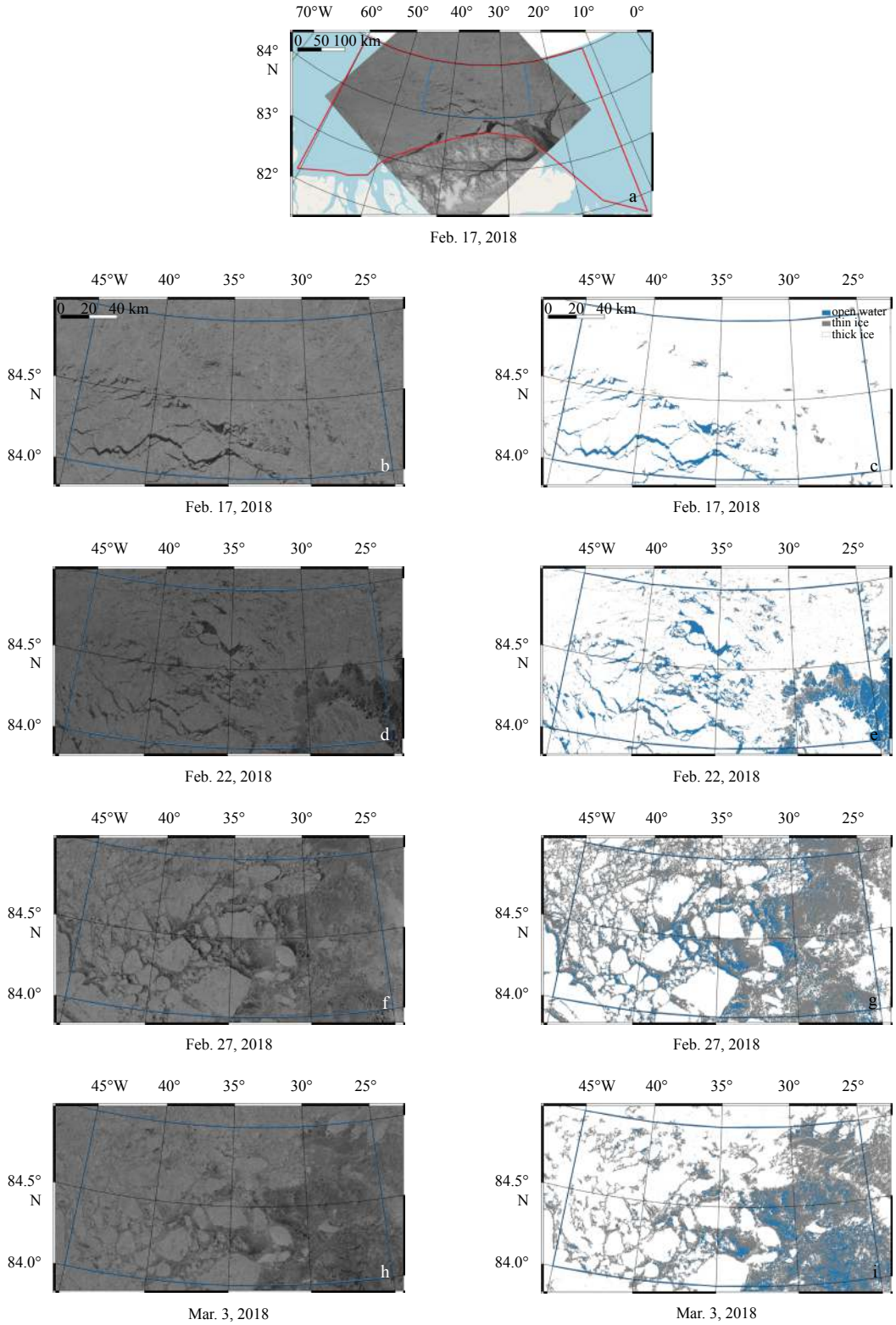

Fig. 3. Original Sentinel-1 SAR images over the study region (red block) and the sub-region (blue block) on selected days during the winter polynya event (a, b, d, f and h), and their corresponding segmented images with three ground objects of thick ice (white), thin new ice (grey), and open water (blue) (c, e, g and i).

Strait, which was much stronger during autumn–spring than in summer (Lei et al., 2016a). During the 2017/2018 ice season, the SLP gradient between the defined points exhibited high variability at the synoptic scale from October 2017 to mid-February 2018, which means that offshore and onshore ice advection alternated. There was a pronounced positive anomaly on December 21, 2017 that was larger than the 1979–2018 climatology by 35 hPa, which indicated stronger onshore wind forcing and ice advection.

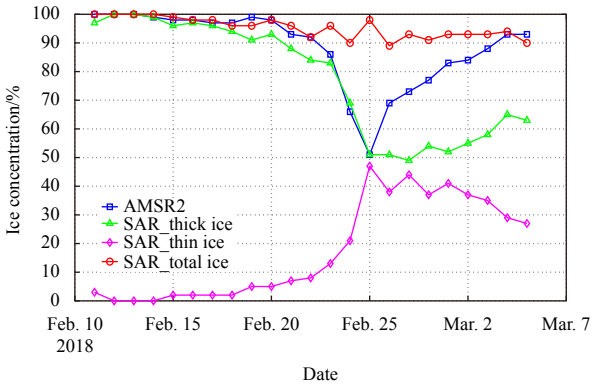

Fig. 4. Changes in sea ice concentration derived from AMSR2 and Sentinel-1 SAR observations from February 11 to March 5, 2018 within sub-region defined in Fig. 3.

However, the synoptic-scale variabilities of the zonal SLP gradient did not result in marked change in the ice concentration within the study region from October 2017 to early February 2018, i.e., it remained >97% until February 16, 2018 (Fig. 2). The ice concentration decreased markedly from then onward because of the rapid reduction in the SLP gradient, which led to strengthened offshore wind forcing and ice advection. During February 11–23, 2018, the SLP gradient dropped by 54 hPa. Because of the strengthened negative phase of the SLP gradient, the ice concentration decreased to 90% by February 19, 2018. The annual lowest SLP gradient (–38 hPa) that occurred on February 23, 2018 was the second lowest throughout 1979–2018. Corresponding to the record low SLP gradient (–40 hPa) that occurred on December 15, 1986, the ice concentration derived from the passive microwave data of the Nimbus-7 Scanning Multichannel Microwave Radiometer (not shown) did not exhibit any identifiable decrease, i.e., the ice concentration remained >95%. This was because that particular occurrence of a low SLP gradient was sustained for only a short time, i.e., the period during which the value was below –15 hPa lasted only five days. The reasonably thick ice cover present in the 1980s (e.g., Lindsay and Schweiger, 2015) also resisted the formation of polynyas because the strength of an ice field is proportional to ice thickness (Hibler, 1979). By the end of the winter polynya event, the SLP gradient increased to a climatological level by March 3, 2018. Combined with the analysis of the SAR images, we can infer that the closure of the polynya was attributed mainly to the formation of new ice and to the stagnation of ice outflow. As shown in Fig. 7, the extremely low SLP gradient during the winter polynya event could have been related to the polar low moving to the north of Greenland and to the high SLP centred over the Barents Sea. Thus, the prevailing wind across the study region was toward the northwest during the winter polynya event.

On July 9, 2018, the SLP gradient decreased to the second lowest during the 2017/2018 ice season because a centre of low SLP occurred over the north of the Canadian Arctic Archipelago and high SLP dominated over Scandinavia. A persistent anomaly of high pressure over Scandinavia caused anomalous high temperatures and drought in that region during summer 2018 (https://www.worldweatherattribution.org/attribution-of-the-2018-heat-in-northern-europe/). The episodic low zonal SLP gradient during July–August 2018 also resulted in a decrease in ice concentration within the study region and it led to the formation of the summer polynya, as shown in Figs 2 and 5. During the summer polynya event, the prevailing wind was also toward the northwest (Figs 7b and c). On August 20, 2018, a pronounced positive abnormal SLP gradient resulted in the increase of ice concentration from then onward. This highlights the contribution of ice inflow from the north to the closure of the polynya.

3.3 *Wind speed and ice flow*

As shown in Fig. 8a, the speed of the northward component of the near-surface wind during February 15–27, 2018 was larger than the 1979–2018 climatology by one standard deviation and this was coincident with the abnormally low zonal SLP gradient shown in Fig. 6. The marked increase in northward ice advection was nearly synchronous with the increased northward wind forcing (Fig. 9a). Although the uncertainty of remote sensing product of ice motion would increase as the decrease in ice concentration and the increase in ice speed (e.g., Sumata et al., 2014) during the polynya event, we argue that its time series was still qualitatively reliable because its temporal change was highly consistent with those of wind forcing and the defined zonal SLP gradient. Based on daily values during the 2017/2018 ice season, the SLP gradient between 90°W and 15°E at 80°N can explain the meridional component of wind across the northern boundary of the study region by 45% (squared value of the correlation coefficient, R^2; P<0.001) and the corresponding meridional component of ice motion by 50% (P<0.001). It implies that our defined zonal SLP gradient constitutes an index that is highly suitable for indicating the meridional component of wind forcing and ice flow to the north of Greenland.

On July 9, 2018, the abnormal low SLP gradient also resulted in an increase in the northward component of the near-surface wind speed (Fig. 8a). The above-average northward wind speed and ice motion, which persisted during July 6–21, 2018 (Figs 8a and 9a), led to the rapid decrease in ice concentration within the study region. Although the northward component of wind forcing was not as strong as during the winter polynya event, the decrease in ice concentration in July 2018 was more obvious (Fig. 2). This was because the increased summer air temperature weakened the consolidation of sea ice and enhanced the response of the sea ice to wind forcing (Hutter et al., 2018). The new ice that formed during the winter polynya event, which might have been reasonably thin because of the short growth period, could have acted as a zone of mechanical vulnerability in summer that encouraged the ice field to break up under the wind forcing. As shown in Fig. 5a, the ice field within the study region on August 1 2018 exhibited a high degree of fragmentation. This would have facilitated lateral melting of the ice floes as the boundaries of the ice floes increased (Steele, 1992). From late July 2018 onward, the meridional components of both wind speed and ice motion exhibited high fluctuation. However, the ice concentration within the study region remained at a low level until the end of August 2018 (Figs 2 and 5). This was because generation of new ice among the floes was prevented by the warm air temperature in summer, as demonstrated by the optical MODIS images (Figs 5a–d). During September 1–19, 2019 (Figs 5e–h), the summer polynya closed gradually because of both the inflow of large floes from the north and the decrease in air temperature as autumn approached.

Across the western and eastern boundaries of the study region, the pattern of wind forcing was similar, i.e., a reasonably strong westward wind during the early period of the winter polynya event and a reasonably strong eastward wind during the late period (Figs 8b and c). Such wind regime would promote ice outflow (inflow) across the western (eastern) boundary during

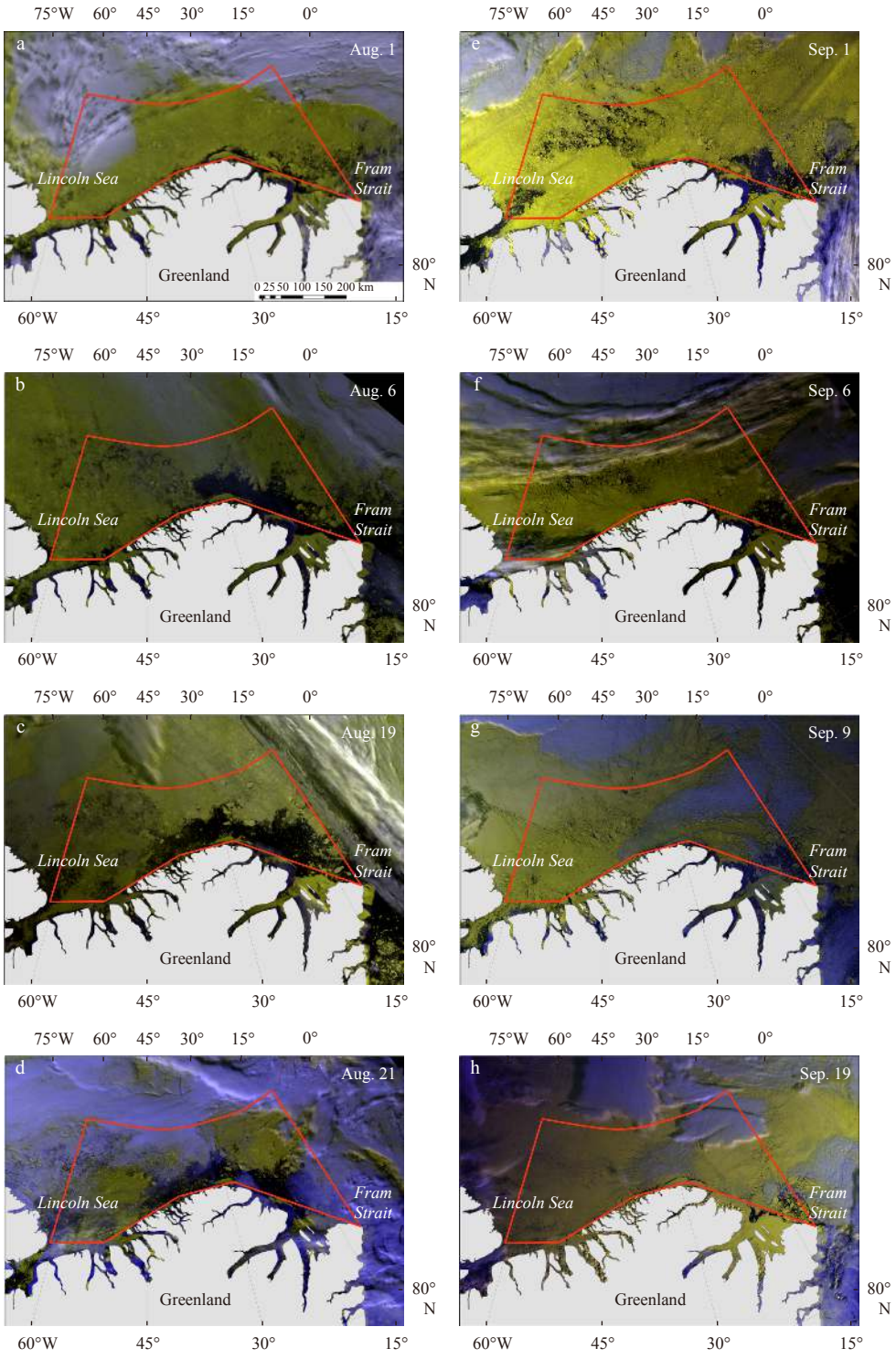

Fig. 5. MODIS images acquired on selected days from August 1 to September 19, 2018. Yellow denotes sea ice, blue and white depict cloud, and dark black indicates open water.

the early part of the winter event, and promote the reversed regime of sea ice advection during the late period (Figs 9b and c). Similar processes also occurred during the summer polynya event.

During the formation stage of the winter polynya (February 13–25, 2018), the average ice outflow across the northern, western, and eastern boundaries based on daily data of AMSR2 ice concentration and NSIDC ice motion was estimated as 2 300 km^2/d, 140 km^2/d and –404 km^2/d (negative means inflow), respectively; during the formation of the summer polynya (July 5 to August 19, 2018), the corresponding values were 389 km^2/d, 123 km^2/d and 90 km^2/d, respectively. Thus, the ice flow across the western and eastern boundaries of the study region played a less important role compared with that across the northern boundary in relation to the formation of the polynya to the north of Greenland, especially for the winter event. During the formation of the sum-

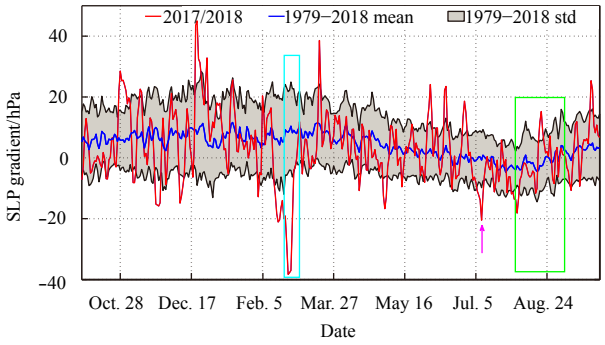

Fig. 6. Time series of daily SLP gradient between 90°W and 15°E at 80°N during the 2017/2018 ice season. Also shown are the 1979–2018 climatology and its standard deviation. Cyan and green rectangles and the purple arrow denote the same events as in Fig. 2.

mer polynya, although the synthetic ice outflow rate across the boundaries was much smaller than the winter case, the accumulated loss of sea ice within the study region was much larger for the summer case because of the relatively long duration of ice loss and the relatively warm air temperature in summer.

3.4 *Near-surface air temperature*

For most of the 2017/2018 ice season, the near-surface air temperature was higher than the 1979–2018 climatology, especially during the period from October 2017 to March 2018. This can be attributed partly to the Arctic Amplification of climate warming, which is more obvious in autumn and winter because of ice-atmosphere feedback (Chylek et al., 2009) and partly to frequent intrusions of extratropical cyclones, which bring warm and moist air from the south (Serreze and Barry, 2011). For example, in late December 2015, the elevation above freezing of the near-surface air temperature at the North Pole was associated with surface cyclones that originated further south (Moore, 2016; Rinke et al., 2017). For our case, the daily zonal SLP gradient from 90°W to 15°E at 80°N can explain the daily near-surface air temperature within the study region by 19% from October 2017 to March 2018 (P<0.01). By setting a filter with an SLP gradient of <0 hPa (34% cases), the R^2 value between the aforementioned two variables increased to 63% (P<0.001). It implies their relationship was more significant under the scenario of the southerly wind. During the winter polynya event, the rapid increase in near-surface air temperature from –28.5°C to –5.2°C during February 10–23, 2018 (Fig. 10) was due to the persistent southerly wind (Fig. 8a). As the southerly wind weakened, the near-surface air temperature declined rapidly to –32.3°C by March 14, 2018. Although the near-surface air temperature during the winter polynya event was much higher than the 1979–2018 climatology, it remained well below the freezing point of seawater. Thus, it could not prevent the production of new ice over open water. Prior to the winter polynya event, the average near-surface air tem-

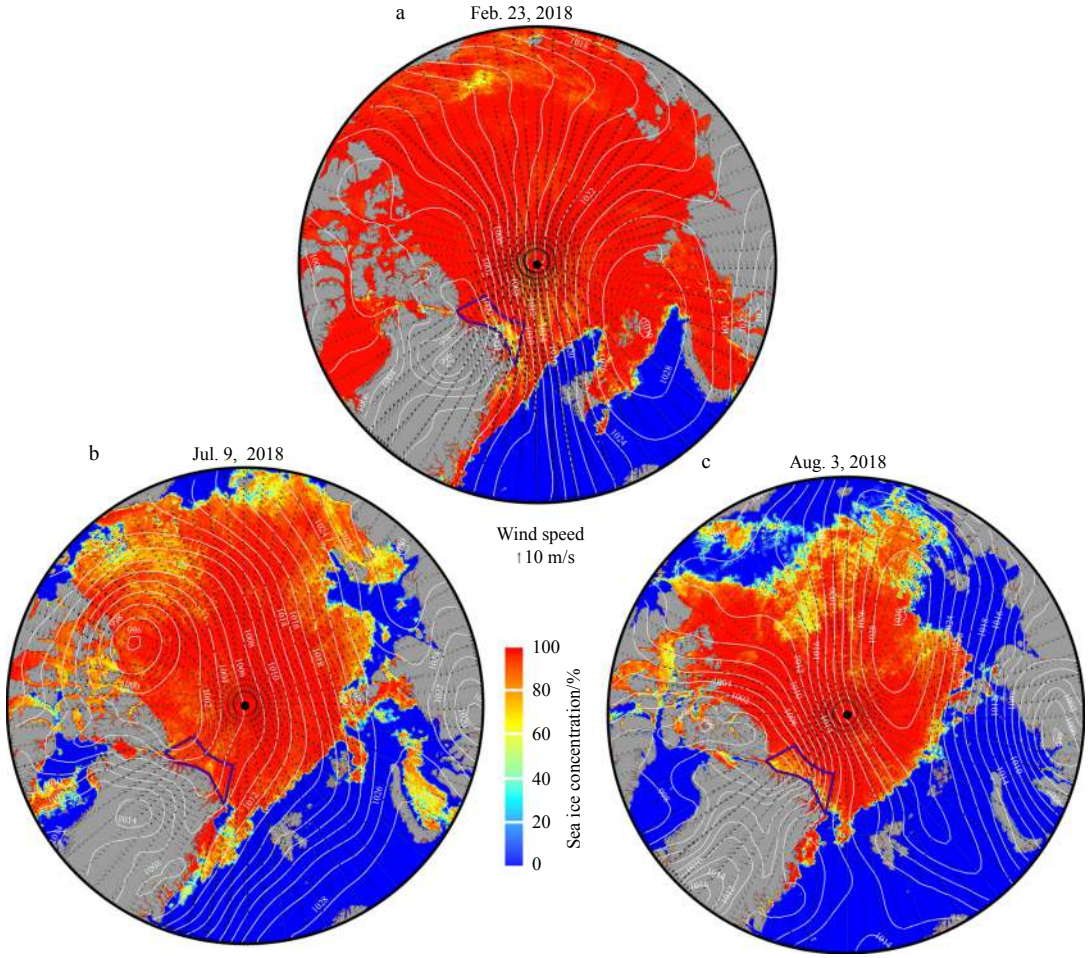

Fig. 7. Contours of SLP and 10-m wind vectors on three selected days. The purple frame delineates the study region.

perature from October 2017 to January 2018 was higher than the 1979–2018 climatology by 3.3 K. Based on an assumed ice thickness of 1.5 m, a simplified analytical model for sea ice thermodynamic growth, which ignores the influence of both snow cover and oceanic heat flux under the ice (Leppäranta, 1993), indicates that basal ice growth would be reduced by 0.13 m by an increase in near-surface air temperature of 3.3 K. Thus, the relatively warm air temperature during the freezing season enhanced the vulnerability of the ice field prior to the winter polynya event. During July–August 2018, the average near-surface air temperature was 1.2°C, i.e., slightly abnormal in comparison with the 1979–2018 climatology (0.3 K). The warm air temperature during summer 2018 prevented new ice production over open water. Thus, the closure of the summer polynya was mainly due to the inflow of ice floes from the north. Ice freezing only made significant impact from the beginning of September 2018 onward, when the air temperature decreased with autumn approaching.

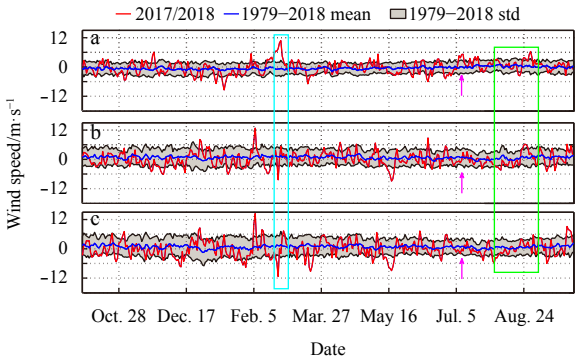

Fig. 8. Meridional component of daily 10-m wind across the northern boundary of the study region (northward is positive) (a); zonal component of daily 10-m wind across the western (b) and eastern (c) boundaries (eastward is positive). Cyan and green rectangles and the purple arrow denote the same events as in Fig. 2.

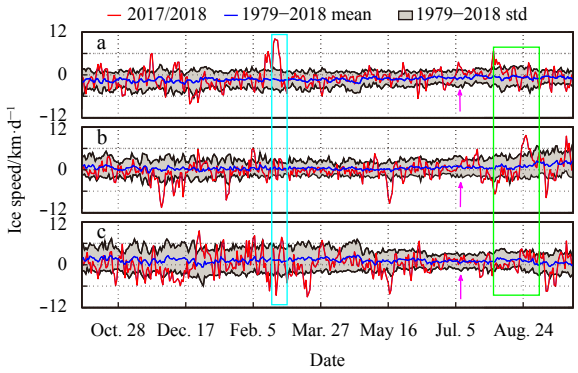

Fig. 9. Meridional component of daily ice motion across thenorthern boundary of the study region (northward is positive) (a); zonal component of daily ice motion across the western (b) and eastern (c) boundaries (eastward is positive). Cyan andgreen rectangles and the purple arrow denote the same events asin Fig. 2.

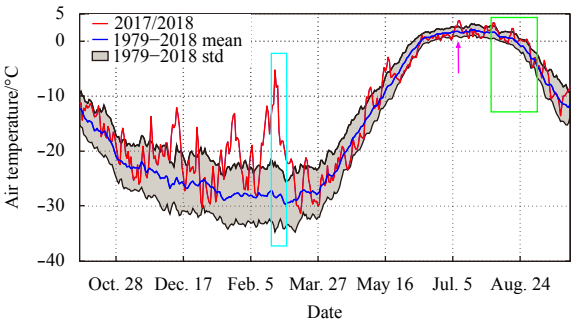

Fig. 10. Time series of daily near-surface air temperature within the study region during the 2017/2018 ice season. Also shown are the 1979–2018 climatology and its standard deviation. Cyan and green rectangles and the purple arrow denote the same events as in Fig. 2.

4 Discussion

4.1 *Relationship to ice outflow through the Fram Strait*

The defined zonal SLP gradient from 90°W to 15°E at 80°N would be influenced by the trajectories of extratropical cyclones moving from the Nordic seas into the Arctic Ocean. When extratropical cyclones move across the Barents Sea or the Fram Strait, they would deepen the SLP over Svalbard and increase the defined SLP gradient. Otherwise, when extratropical cyclones propagate into areas to the northwest of Greenland, e.g., the Canadian Arctic Archipelago, they would decrease the defined SLP gradient. In the climatology, the extreme cyclone events occur more frequently over the Svalbard than in the regions to the northwest of Greenland during the winter (Rinke et al., 2017). Thereby, the extreme negative zonal SLP gradient observed in mid- and later February 2018 (Fig. 6) can be considered as an extremely unusual event from the perspective of the impact of cyclone behaviors. However, the increased trend of winter cyclone activities over Canadian Arctic Archipelago and the opposite trend over the Kara Sea and Barents Sea (Rinke et al., 2017) would have potential to increase the south wind across the north Greenland. This, associated with the warming surface air temperature, and the loss of multiyear ice and the thinning of ice thickness over the Arctic Ocean, would increase the probability of polynya event north of Greenland, which makes it no longer an isolated event.

The most prominent atmospheric driver of sea ice motion across the Fram Strait is the east-west SLP gradient between the Barents Sea and Greenland (Tsukernik et al., 2010). Ice advection from the central Arctic Ocean to the Fram Strait along the Transpolar Drift Stream (TDS) can be related to the east-west SLP gradient between 90°W and 90°E at 84°N (Vihma et al., 2012; Lei et al., 2019). Taking February as an example, the R^2 value between the monthly zonal SLP gradient defined in this study and the SLP gradient between 90°W and 90°E at 84°N is 0.18 (P<0.01) in 1979–2018; and that between our defined SLP gradient and that defined by Tsukernik et al. (2010) is 0.67 (P<0.001) in 1979–2018. It implies that the meridional component of ice motion north of Greenland is likely to exhibit significant consistency with ice advection along the TDS, especially for ice motion across the Fram Strait. The abnormal southerly wind to the north of Greenland during the polynya event in February 2018 is associated with a weakened TDS and reduced ice outflow through the Fram Strait. In February and July 2018, during the formation of the winter and summer polynyas, the meridional component of the 10-m wind speed at the centre of the Fram Strait (80°N, 0°W) was 1.5 m/s and 2.5 m/s (positive value means toward the north), respectively, which contrasts sharply with the 1979–2018 climatology values of −4.0 m/s and 0.1 m/s, respectively. It implies that

surface wind forcing weakened ice outflow through the Fram Strait during the formation of the winter and summer polynyas.

4.2 *Relationship to the mid-troposphere polar vortex*

The evolution of the 500-hPa geopotential height can be used to indicate the perturbation of the mid-troposphere polar vortex (Moore, 2016). Perturbation of the mid-tropospheric flow can have significant influence on the intrusion of moist air masses and extratropical cyclones into the Arctic Ocean (Rinke et al., 2017). During February 5–23, 2018, a trough of 500-hPa geopotential height extended southeastwardly to the Iceland Basin. The corresponding ridge extended northward to the Barents Sea or even further north, as did the jet stream (Figs 11a and d). On February 23, 2018, the leading edge of the ridge of geopotential height reached the North Pole. Thus, during this event, warm air masses intruding into the Arctic could not be pushed back by the mid-troposphere polar vortex, which is a "wall" of wind that circulates the Arctic region. At the extreme, the near-surface air temperature to the north of Greenland in February 2018 increased to 23 K above the 1979–2018 climatology. The ERA-Interim product indicates that such sharp warming of surface air was not restricted locally but spanned almost the entire Arctic Ocean (data not shown). Thereby, it would markedly reduce Arctic ice growth. The long-team time series in 1958–2015 also indicates that the extreme warm events show a significant increase trend over the region near the North Pole (Moore, 2016).

In summer, the mid-troposphere polar vortex was nearly collapsed with a weakened upper-level low-pressure field of air rotating around the North Pole. However, the dipole pattern of 500-hPa geopotential height characterized by relatively low and high geopotential height to the west and east of Greenland, respectively, was still distinct on both July 9 and August 3, 2018 (Figs 11e and f). Thereby, the perturbation of the mid-troposphere polar vortex and the amplified planetary wave over the Nordic seas played important roles in the enhancement of the surface southerly wind and the formation of the polynyas to the north of Greenland in both February and July 2018. As shown in Fig. 12, during both the winter and the summer polynya events, change in the daily SLP gradient between 90°W and 15°E at 80°N was almost synchronous with that in the difference of 500-hPa geopotential height between these two sites. It implies the surface wind changed nearly with the same rhythm as the mid-troposphere winds, without any identifiable delay.

4.3 *Influence on the NOW polynya*

To assess the influence of the winter polynya event north of Greenland on ice condition in regions related to the NOW polynya, we calculated the spatial average ice concentration in nine defined blocks. As shown in Fig. 13a, Blocks 1–8 stretch from Lincoln Sea southward into Baffin Bay. They are divided quasi-equidistantly in the meridional direction and following the coastline trend of the Nares Strait. Block 1 comprised the area south of the Lincoln Sea and close to the northern entrance of the Nares

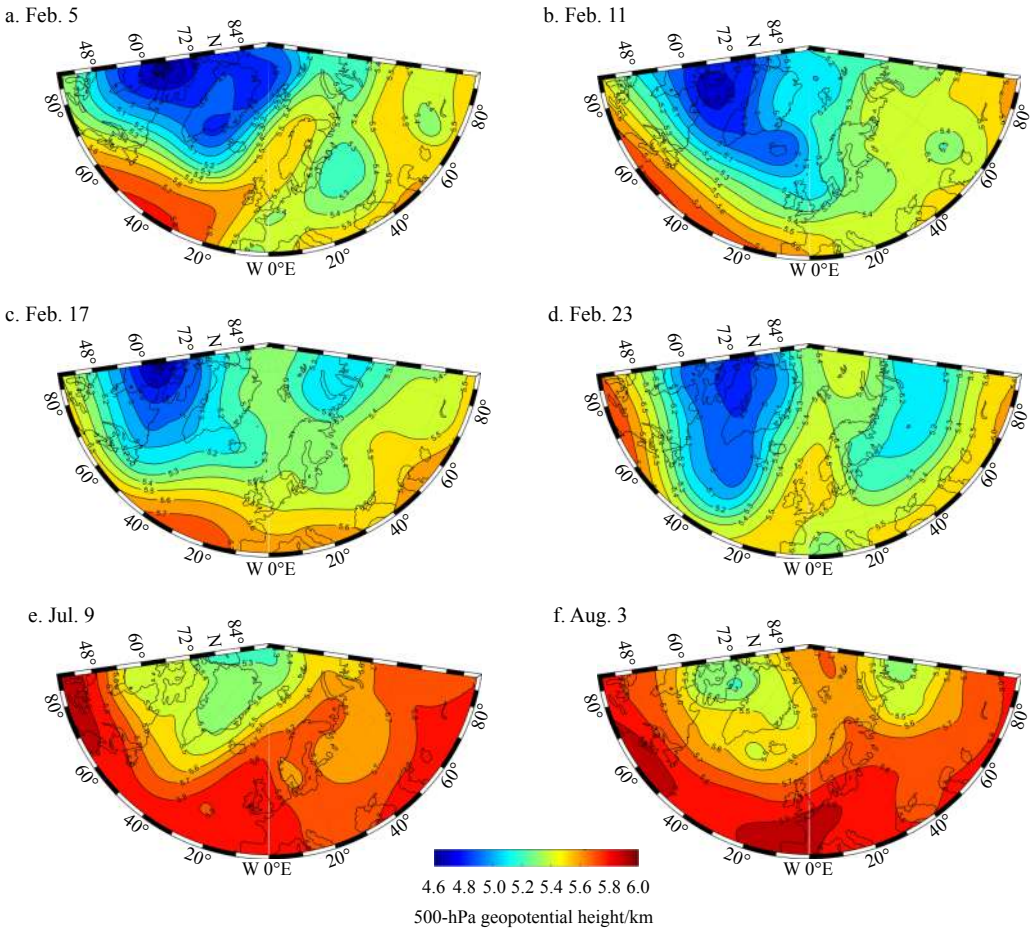

Fig. 11. Evolution of 500-hPa geopotential height during the formation stage of the winter polynya (a–d) and the summer polynya (e–f) in the Atlantic sector from 40°–90°N.

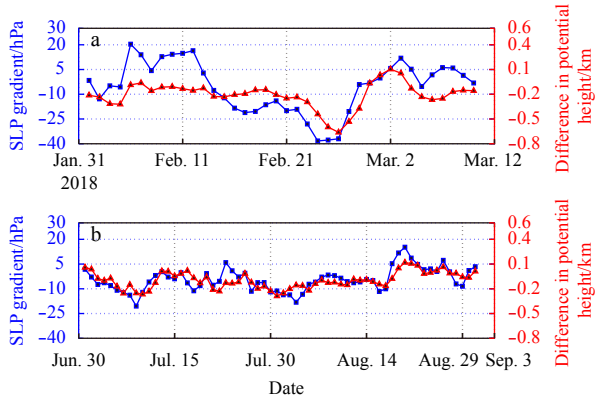

Fig. 12. Change in the daily SLP gradient and in the difference in 500-hPa geopotential height between 90°W and 15°E at 80°N during the winter (a) and summer (b) polynya events.

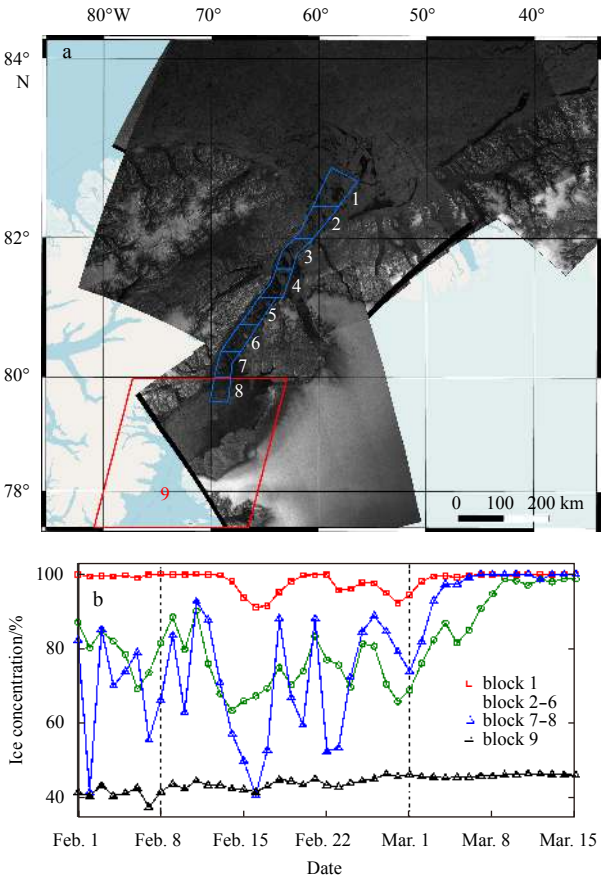

Fig. 13. Sentinel-1 SAR image over the Lincoln Sea and the Nares Strait on February 17, 2018 (a); and change in AMSR2 ice concentration in different blocks from north to south in February 2018 (b).

Strait. Block 2–6 covered regions within the Nares Strait; Blocks 7–8 encompassed the southern entrance of the Nares Strait, and Block 9 comprised the north of Baffin Bay and also the northern part of the NOW polynya (Tamura and Ohshima, 2011). As shown in Fig. 13a, during the winter polynya event north of Greenland, the ice field was broken up in the Lincoln Sea on February 17, 2018, which strengthened ice mobility and resulted in the disappearance of the ice bridge across the northern entrance of the Nares Strait. The ice concentration in Block 1 decreased markedly in two distinct episodic periods: February 15–19 and February 23, to March 1, 2018, which indicated the breakup of the ice bridge in the south of the Lincoln Sea. The change in ice concentration in Blocks 2–6 along the Nares Strait was similar to that in Block 1 but it exhibited greater fluctuation. It implies the Nares Strait was unblocked for ice advection during the winter polynya event north of Greenland. The ice concentration increased markedly from March 1 onward as the wind forcing turned toward the south. The Nares Strait was nearly closed from north to south by March 9, 2018. In the northern part of the NOW polynya region (Block 9), the ice concentration increased slightly from February 16, to March 1, 2018, which was likely attributable to ice inflow from the Nares Strait. From then onward, the ice concentration in this region remained unchanged. It implies that the winter polynya event north of Greenland and the associated atmospheric forcing led to the breakup of the ice bridge to the north of the NOW polynya and to a slight increase in ice concentration in the NOW polynya region. However, such event did not result in the closure of the NOW polynya because the event lasted for only a short period and the ice bridge was re-established in the Nares Strait by mid-March 2018. Thereby, the influence of the winter polynya event north of Greenland on the NOW polynya was temporary and very limited.

5 Conclusions

Two polynya events occurred during the 2017/2018 ice season in a region to the north of Greenland, where the oldest and thickest ice within the Arctic Ocean is expected to exist. A threshold ice concentration of 90% revealed the winter polynya event lasted from February 20 to March 3, 2018 and the summer event persisted from August 2 to September 5, 2018. Based on AMSR2 data, it was established that the minimum spatially averaged ice concentration within the study region during the winter and summer polynya events was 72% and 65%, respectively, both of which were also the minimum values for the freezing season and the melt season during 2002–2018. Both the winter and summer polynyas north of Greenland were the unprecedented events in the era of remote sensing observation, which are different from most polynyas in other regions of Arctic, e.g., those along the shore of Russia, in the north of Baffin Bay, on the southern coast of St. Lawrence Island, which have relatively strong reproducibility because the ice in these regions has relatively high mobility and better responsiveness to wind forcing (Tamura and Ohshima, 2011). Here, we argue that the reproducibility of polynya event north of Greenland would be enhanced as the climate warming and the thinning of sea ice, as well as the increased intrusions of strong extratropical cyclones over the Arctic Ocean (e.g., Rinke et al., 2017). The intrusions of extratropical cyclones could promote the northward advection of warm air masses and the generation of strong southerly winds in certain special regions.

Both polynya events can be related to the strengthened southerly wind associated with the increased zonal SLP gradient between Svalbard and the area to the north of Ellesmere Island. Thus, the polynyas can be categorized as latent-heat polynyas, whose formation is associated with the land bridge in the upstream area of the wind. Therefore, its formation and development mechanisms summarized in this study are similar with the latent-heat polynyas in other Arctic regions, e.g., that on the southern coast of St. Lawrence Island (Barber and Massom, 2007).

The mid-troposphere polar vortex acts as a barrier that isolates Arctic air from the intrusion of warmer air from the south.

Thus, variations in the polar vortex can cause disruption in expected weather patterns across the Northern Hemisphere. Both polynya events identified in this study can be related to perturbation of the mid-troposphere polar vortex. The anomalous southerly wind brought moist and warm air masses from the south, while the retreat of the mid-troposphere polar vortex in the section of the Nordic seas weakened its ability to block the northward invasion of moist and warm air masses from the south. During the winter polynya event, the maximum anomaly of the near-surface air temperature reached 23 K relative to the 1979–2018 climatology. The meridional component of wind forcing across the study region was significantly correlated with that across the Fram Strait. Thus, the formation of the polynyas in the region to the north of Greenland was related to the reduced Arctic sea ice outflow through the Fram Strait.

Although the air temperature was reasonably high during the winter polynya event, it still could not prevent the formation of new ice over the polynya. For example, new ice developed over 47% of the area of open water in the central part of the study region, which was comparable with the area of background thick ice. The thin new ice was almost impossible to be identified in the initial stage using the AMSR2 observations. Thus, passive microwave observations have limited capacity with regard to the estimation of ice production during polynya events. The increase in both the thickness and the area of new ice, as well as the weakened southerly wind, played crucial roles in the closure of the winter polynya. The winter polynya event and the associated atmospheric forcing led to the breakup of the ice bridge to the north of the NOW polynya.

At the beginning of the summer polynya event during early August 2018, the ice floes exhibited a high degree of fragmentation. It is likely that the winter polynya event contributed to the breakup of sea ice in summer through the creation of zones of mechanical vulnerability related to the new ice. Associated with the reasonably warm air temperature in summer, lateral melt of ice floes was likely to have promoted the development of the polynya. Thereby, the maximum area fraction of open water within the study region during the summer polynya event was much larger than in the winter event, even though the southerly wind was relatively weak in summer. In early September 2018, the inflow of large floes from the north and the decreased air temperature were the major factors contributing to the closure of the summer polynya.

The unprecedented polynya events in the region to the north of Greenland during the 2017/2018 ice season are noteworthy from the perspective of Arctic sea ice loss because they occurred in a region in which the thickest and oldest sea ice within the Arctic Ocean is expected to exist. It is considered that this region could potentially be the last “Arctic sea ice refuge” in future summers (Overland and Wang, 2013). Since polynya events can also appear over such region, we expect that the polynya events would regularly appear as the continuous thinning of Arctic sea ice.

Acknowledgements

The AMSR2 passive microwave ice concentrations were provided by the University of Bremen. The ice motion product was provided by the NSIDC. The MODIS optical images and Sentinel-1 SAR images were provided by the NASA and the ESA, respectively. The ERA-Interim reanalysis was obtained from the ECMWF.

References

Barber D G, Massom R A. 2007. The role of sea ice in Arctic and Antarctic polynyas. In: Smith W O Jr, Barber D G, eds. Polynyas: Windows to the World, Elsevier Oceanography Series, Vol. 74. Amsterdam: Elsevier, 1–54

Cavalieri D J, Martin S. 1994. The contribution of Alaskan, Siberian, and Canadian coastal polynyas to the cold halocline layer of the Arctic Ocean. Journal of Geophysical Research, 99(C9): 18343–18362, doi: 10.1029/94JC01169

Chylek P, Folland C K, Lesins G, et al. 2009. Arctic air temperature change amplification and the Atlantic Multidecadal Oscillation. Geophysical Research Letters, 36(14): L14801, doi: 10.1029/2009GL038777

Comiso J C, Gordon A L. 1996. Cosmonaut polynya in the southern ocean: structure and variability. Journal of Geophysical Research, 101(C8): 18297–18313, doi: 10.1029/96JC01500

Dee D P, Uppala S M, Simmons A J, et al. 2011. The ERA-Interim reanalysis: Configuration and performance of the data assimilation system. Quarterly Journal of the Royal Meteorological Society, 137(656): 553–597, doi: 10.1002/qj.828

Dierking W. 2010. Mapping of different sea ice regimes using images from Sentinel-1 and ALOS synthetic aperture radar. IEEE Transactions on Geoscience and Remote Sensing, 48(3): 1045–1058, doi: 10.1109/TGRS.2009.2031806

Dierking W. 2013. Sea ice monitoring by synthetic aperture radar. Oceanography, 26(2): 100–111

Dmitrenko I A, Kirillov S A, Rysgaard S, et al. 2015. Polynya impacts on water properties in a Northeast Greenland fjord. Estuarine, Coastal and Shelf Science, 153: 10–17, doi: 10.1016/j.ecss.2014.11.027

Dmitrenko I A, Tyshko K N, Kirillov S A, et al. 2005. Impact of flaw polynyas on the hydrography of the Laptev Sea. Global and Planetary Change, 48(1–3): 9–27, doi: 10.1016/j.gloplacha.2004.12.016

Else B G T, Papakyriakou T N, Asplin M G, et al. 2013. Annual cycle of air-sea CO_2 exchange in an Arctic polynya region. Global Biogeochemical Cycles, 27(2): 388–398, doi: 10.1002/gbc.20016

Gallée H. 1997. Air-sea interactions over Terra Nova Bay during winter: Simulation with a coupled atmosphere-polynya model. Journal of Geophysical Research: Atmospheres, 102(D12): 13835–13849, doi: 10.1029/96JD03098

Gutjahr O, Heinemann G, Preußer A, et al. 2016. Quantification of ice production in Laptev Sea polynyas and its sensitivity to thin-ice parameterizations in a regional climate model. The Cryosphere, 10(6): 2999–3019, doi: 10.5194/tc-10-2999-2016

Hibler W D III. 1979. A dynamic thermodynamic sea ice model. Journal of Physical Oceanography, 9(4): 815–846, doi: 10.1175/1520-0485(1979)009<0815:ADTSIM>2.0.CO;2

Hong D B, Yang C S. 2018. Automatic discrimination approach of sea ice in the Arctic Ocean using Sentinel-1 Extra Wide Swath dual-polarized SAR data. International Journal of Remote Sensing, 39(13): 4469–4483, doi: 10.1080/01431161.2017.1415486

Hutter N, Losch M, Menemenlis D. 2018. Scaling properties of Arctic sea ice deformation in a high-resolution viscous-plastic sea ice model and in satellite observations. Journal of Geophysical Research, 123(1): 672–687

Kimura N, Nishimura A, Tanaka Y, et al. 2013. Influence of winter sea-ice motion on summer ice cover in the Arctic. Polar Research, 32(1): 20193, doi: 10.3402/polar.v32i0.20193

Krumpen T, Hölemann J A, Willmes S, et al. 2011. Sea ice production and water mass modification in the eastern Laptev Sea. Journal of Geophysical Research, 116(C5): C05014

Kwok R. 2005. Ross Sea ice motion, area flux, and deformation. Journal of Climate, 18(18): 3759–3776, doi: 10.1175/JCLI3507.1

Lange B A, Beckers J F, Casey J A, et al. 2019. Airborne observations of summer thinning of multiyear sea ice originating from the Lincoln Sea. Journal of Geophysical Research, 124(1): 243–266

Lei Ruibo, Gui Dawei, Hutchings J K, et al. 2019. Backward and forward drift trajectories of sea ice in the northwestern Arctic Ocean in response to changing atmospheric circulation. International Journal of Climatology, 39(11): 4372–4391, doi: 10.1002/joc.6080

Lei Ruibo, Heil P, Wang Jia, et al. 2016a. Characterization of sea-ice

kinematic in the Arctic outflow region using buoy data. Polar Research, 35(1): 22658, doi: 10.3402/polar.v35.22658

Lei Ruibo, Tian-Kunze X, Leppäranta M, et al. 2016b. Changes in summer sea ice, albedo, and portioning of surface solar radiation in the Pacific sector of Arctic Ocean during 1982–2009. Journal of Geophysical Research: Oceans, 121(8): 5470–5486, doi: 10.1002/2016JC011831

Leppäranta M. 1993. A review of analytical models of sea-ice growth. Atmosphere-Ocean, 31(1): 123–138, doi: 10.1080/07055900.1993.9649465

Lindsay R, Schweiger A. 2015. Arctic sea ice thickness loss determined using subsurface, aircraft, and satellite observations. The Cryosphere, 9(1): 269–283, doi: 10.5194/tc-9-269-2015

Martin S. 2001. Polynyas. In: Steele J H, ed. Encyclopedia of Ocean Sciences. 2nd ed. San Diego: Academic Press, 540–545

Martin S, Drucker R, Kwok R, et al. 2005. Improvements in the estimates of ice thickness and production in the Chukchi Sea polynyas derived from AMSR-E. Geophysical Research Letters, 32(5): L05505

Maykut G A. 1982. Large-scale heat exchange and ice production in the central Arctic. Journal of Geophysical Research, 87(C10): 7971–7984, doi: 10.1029/JC087iC10p07971

Moore G W K. 2016. The December 2015 North Pole warming event and the increasing occurrence of such events. Scientific Reports, 6(1): 39084, doi: 10.1038/srep39084

Moore G W K, Schweiger A, Zhang J, et al. 2018. What caused the remarkable February 2018 North Greenland Polynya?. Geophysical Research Letters, 45(24): 13342–13350, doi: 10.1029/2018GL080902

Morales Maqueda M A, Willmott A J, Biggs N R T. 2004. Polynya dynamics: A review of observations and modeling. Reviews of Geophysics, 42(1): RG1004

Ohshima K I, Nihashi S, Iwamoto K. 2016. Global view of sea-ice production in polynyas and its linkage to dense/bottom water formation. Geoscience Letters, 3(1): 13, doi: 10.1186/s40562-016-0045-4

Overland J E, Wang M Y. 2013. When will the summer Arctic be nearly sea ice free?. Geophysical Research Letters, 40(10): 2097–2101, doi: 10.1002/grl.50316

Rinke A, Maturilli M, Graham R M, et al. 2017. Extreme cyclone events in the Arctic: Wintertime variability and trends. Environmental Research Letters, 12(9): 094006, doi: 10.1088/1748-9326/aa7def

Serreze M C, Barry R G. 2011. Processes and impacts of Arctic amplification: a research synthesis. Global and Planetary Change, 77(1–2): 85–96, doi: 10.1016/j.gloplacha.2011.03.004

Spreen G, Kaleschke L, Heygster G. 2008. Sea ice remote sensing using AMSR-E 89-GHz channels. Journal of Geophysical Research, 113(C2): C02S03

Steele M. 1992. Sea ice melting and floe geometry in a simple ice-ocean model. Journal of Geophysical Research, 97(C11): 17729–17738, doi: 10.1029/92JC01755

Sumata H, Lavergne T, Girard-Ardhuin F, et al. 2014. An intercomparison of Arctic ice drift products to deduce uncertainty estimates. Journal of Geophysical Research: Oceans, 119(8): 4887–4921, doi: 10.1002/2013JC009724

Sumata H, Kwok R, Gerdes R, et al. 2015. Uncertainty of Arctic summer ice drift assessed by high-resolution SAR data. Journal of Geophysical Research: Oceans, 120(8): 5285–5301, doi: 10.1002/2015JC010810

Tamura T, Ohshima K I. 2011. Mapping of sea ice production in the Arctic coastal polynyas. Journal of Geophysical Research, 116(C7): C07030

Tsukernik M, Deser C, Alexander M, et al. 2010. Atmospheric forcing of Fram Strait sea ice export: A closer look. Climate Dynamics, 35(7): 1349–1360

Vihma T, Tisler P, Uotila P. 2012. Atmospheric forcing on the drift of Arctic sea ice in 1989–2009. Geophysical Research Letters, 39(2): L02501